Vänskä, Osmo; Tittonen, Ilkka; Koch, Stephan; Kira, Mackillo

Coherent Terahertz Control of Vertical Transport in Semiconductor Heterostructures

Published in:
Physical Review Letters

DOI:
10.1103/PhysRevLett.114.116802

Published: 01/01/2015

Document Version
Publisher's PDF, also known as Version of record

Please cite the original version:
Vänskä, O., Tittonen, I., Koch, S., & Kira, M. (2015). Coherent Terahertz Control of Vertical Transport in Semiconductor Heterostructures. *Physical Review Letters*, *114*(11), 116802-116806.
https://doi.org/10.1103/PhysRevLett.114.116802

Coherent Terahertz Control of Vertical Transport in Semiconductor Heterostructures

O. Vänskä,[1,2,*] I. Tittonen,[1] S. W. Koch,[2] and M. Kira[2]
[1]Department of Micro- and Nanosciences, Aalto University, P.O. Box 13500, FI-00076 Aalto, Finland
[2]Department of Physics and Material Sciences Center, Philipps-Universität Marburg, Renthof 5, 35032 Marburg, Germany
(Received 2 June 2014; published 16 March 2015)

Coherent-control protocols are introduced to selectively transport electrons, excitons, or pure two-particle correlations through semiconductor interfaces. The scheme is tested in a double-quantum-well structure where a sequence of terahertz pulses is applied to induce the vertical excitation transfer between the wells. Using a microscopic theory, it is shown that efficient and highly selective transfer can be realized even in the presence of the unavoidable scattering and dephasing processes.

DOI: 10.1103/PhysRevLett.114.116802 PACS numbers: 73.40.Kp, 71.35.Gg, 78.67.De

The ultrafast optical generation of photocurrents has attracted considerable attention over the past few years [1–5]. Using a coherent control scheme of two short coherent light pulses with central frequencies ω and $\omega/2$, it has been possible to induce electric currents not only in semiconductors but also on metal surfaces where ultrafast dephasing processes are omnipresent [6]. Besides the transport of real charge carriers, it was also possible to generate pure spin currents in semiconductors by choosing linear perpendicular polarizations of the two beams [7,8]. Here, the electrons with opposite spins flow into opposite directions resulting in a net spin transport without changing the local charge-carrier density.

As successful as these coherent optical schemes have been, they could only be used to generate currents in homogeneous systems; i.e., they do not involve any vertical transport across interfaces. Vertical transport, however, is of crucial importance for many systems and devices. For example, the functionality of solar cells depends on the selective transport of electrons and holes at semiconductor interfaces [9,10]. All tunnel-junction single-electron devices are based on the control of electron transport through material barriers [11]. Likewise, the operational principle of the quantum cascade laser involves efficient electron transport vertically through multiple quantum-well (QW) layers [12,13]. Even biological processes, such as photosynthesis, involve the electron transport through internal boundaries [14,15].

To study the fundamental properties of vertical transport, it is desirable to have a coherent control scheme that makes it possible to selectively transfer charges, charge clusters, or even particular correlation properties through interfaces. In this Letter, we develop vertical-transport protocols that utilize sequences of terahertz (THz) pulses and can be applied to a wide variety of semiconductor heterostructures. As a model system, we use a type-II double-QW structure where the hole remains fixed in one of the wells, while the electrons can be moved between the QWs. We demonstrate that a sequence of THz pulses can selectively transport either an electron plasma or bound electron-hole pairs (excitons) so precisely that we cannot only induce the selective electron or exciton transport but even design a protocol where *only* pure exciton correlations are transferred across the internal interface. In other words, neither electrons nor excitons are transported in this case; only the correlations move through the double-QW interfaces. We show that the pure exciton-correlation transport is detectable by monitoring the time-resolved photoluminescence.

The principle scheme for the coherent THz-induced vertical transport is illustrated in Fig. 1. We consider a GaAs-based double-QW with type-II band alignment shown schematically in Fig. 1(a). The left (right) QW is 4 nm (5 nm) thick, and the QWs are separated by a 4-nm-thick tunneling barrier; the exact material parameters are provided in Ref. [16]. The idea behind this structural design is the realization of a configuration where the lowest-energy excited electron-hole pair is indirect, with the hole (electron) confined to the left (right) QW, whereas the first excited electron-hole state is direct.

We consider optical excitation conditions that predominantly generate electrons and holes or type-I excitons in the left QW. After the optical excitations, these states will relax into a type-II configuration. The ground state is then a type-II or charge-transfer exciton where the electron and hole are spatially separated, which yields significant reduction in recombination rates and photoluminescence [22]. The tunneling barrier between the QWs ensures that the relaxation is slow enough such that direct excitons may also exist for a sufficiently long time. Because of the differences in the electronic confinement functions, the binding energies of direct and indirect excitons are different. For our parameters, the energy separation of these excitons corresponds to a different THz frequency $\nu_X = 3.6$ THz than the electronic $\nu_e = 4.8$ THz transition frequency [16].

In all cases, we assume that the THz field has a propagation (polarization) direction along (perpendicular to) the QW plane such that the THz-induced transitions produce a vertical transport of electrons between the

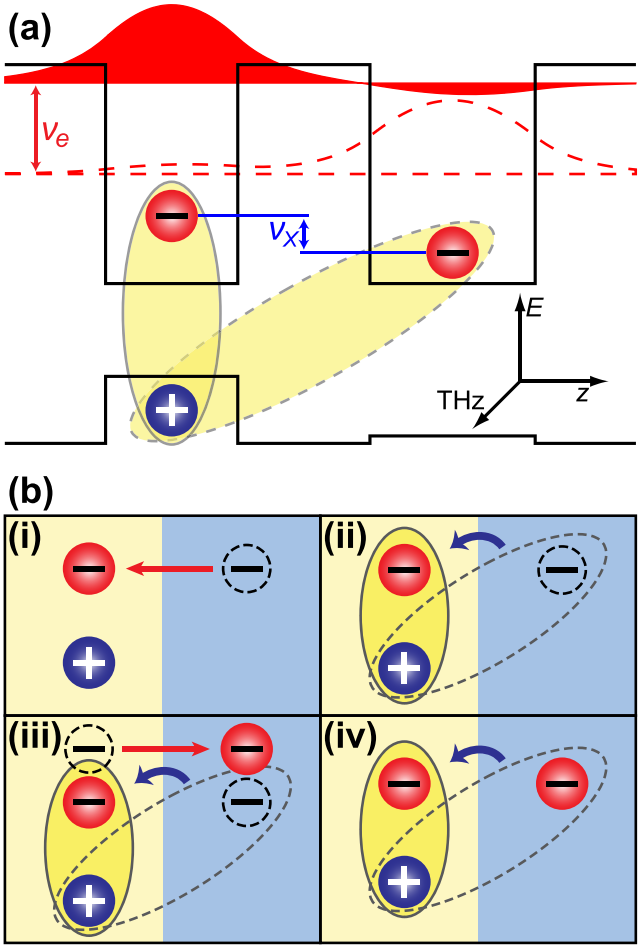

FIG. 1 (color online). Setup for vertical electron transport. (a) Schematic configuration of the conduction- and valence-band edges of a double-QW structure with type-II band alignment. Here, the energetically lowest unbound electron-hole pair is indirect (electrons in the right and holes in the left QW). The next higher unbound electron-hole-pair state is direct (type-I) and separated from the indirect (type-II) state by the transition frequency $\nu_e = 4.8$ THz. The corresponding bound exciton states are separated by the frequency $\nu_X = 3.6$ THz. (b) Schematic presentation of protocols. While holes (blue spheres) remain in the left QW, electrons (red spheres) move through the interface, yielding (i) electron, (ii) exciton, and (iii) pure exciton-correlation transport. The dashed symbols denote the initial state, and arrows identify the transitions; the net effect of protocol (iii) is summarized in frame (iv).

excited and ground states without changing the electron-hole symmetry in the in-plane direction [16,23], unlike for the perpendicular propagation direction [24]. When the THz frequency matches ν_e or ν_X, pure plasma or exciton-bound electron transport is expected, respectively. Since ν_e and ν_X are significantly different, we can expect a high degree of transport selectivity simply by changing the frequency of the THz field.

Different schemes of the THz-induced vertical transport scenarios are shown in Fig. 1(b). Generally, the electrons (red spheres) can be on either side of the interface, whereas the holes (blue spheres) remain in the left region (light area). The excitons are symbolized by the yellow ellipses representing the electron-hole correlation. The dashed symbols identify the initial type-II states. Pure electron transport is achieved when an uncorrelated electron is moved from right to left, as depicted Fig. 1(b)(i). Figure 1(b)(ii) present exciton transport where the electron part of the exciton is moved through the interface. To realize the transport of pure exciton correlations across the interface, we consider an initial condition where excitons are in the right region and free electrons are in the left region, respectively. As long as the electron- and exciton-transport protocols are sufficiently selective, we can apply them simultaneously in order to produce the processes identified in Fig. 1(b)(iii). Since the transport merely interchanges the positions of the unbound and bound electrons, the net result does not change the local electron populations but rather yields the pure correlation transport summarized in Fig. 1(b)(iv). In other words, with a suitably prepared initial state and the proper transport protocol, one should be able to effectively move pure exciton correlations across the interface without net particle transport. In many ways, this scenario is analogous to the generation of pure spin currents in the coherent optical control schemes mentioned above.

For our microscopic modeling of the proposed transport protocols, we start from a general system Hamiltonian including the Coulomb coupling among the electrons and holes as well as the optical and THz interactions in the $\mathbf{E}\cdot\mathbf{r}$ picture [16]. This approach yields a fully microscopic description of the relevant THz-field-induced many-body effects which are treated using the cluster-expansion method [25,26]. To solve the quantum kinetics excited by the THz-transport protocols, we need to evolve the dynamics of several observables, including the microscopic electron occupation $f_{\mathbf{k}}^{e,\lambda}$, where $\hbar\mathbf{k}$ is the crystal momentum of an electron at confinement level λ. In our case, $\lambda = L$ ($\lambda = R$) refers to electrons in the left (right) QW. The corresponding hole occupation is $f_{\mathbf{k}}^{h,L}$, and the intersubband polarization between electronic bands is defined by $p_{\mathbf{k}}^{\lambda,\lambda'}$ with $\lambda' \neq \lambda$. Excitons are described by a true two-particle correlation $C_{\lambda,\lambda'}^{\mathbf{q},\mathbf{k}',\mathbf{k}}$ between an electron and a hole with a center-of-mass (relative) momentum $\hbar\mathbf{q}$ ($\hbar\mathbf{k}$ or $\hbar\mathbf{k}'$) and electron positions (λ,λ') across the interface. Only $\lambda = \lambda'$ defines a true exciton correlation, whereas $\lambda \neq \lambda'$ represents a correlated transition amplitude for moving an electron through the barrier. All optically induced interband coherences are assumed to have decayed because we study the THz-induced transport long after the optical excitation.

For sufficiently dilute carrier densities, the cluster expansion produces a closed set of singlet-doublet equations [16,25]

$$\hbar\frac{\partial}{\partial t}f_{\mathbf{k}}^{e,\lambda}=2\mathrm{Im}\left[(\Omega_{\mathbf{k}}^{\lambda})^{*}p_{\mathbf{k}}^{\lambda,\bar{\lambda}}+\sum_{\mathbf{q}}V_{\lambda,\lambda}^{\mathbf{q},\mathbf{k}-\mathbf{q},\mathbf{k}}\right], \quad (1)$$

$$\hbar\frac{\partial}{\partial t}f_{\mathbf{k}}^{h,L}=2\sum_{\lambda,\mathbf{q}}\mathrm{Im}[V_{\lambda,\lambda}^{\mathbf{q},\mathbf{k},\mathbf{k}+\mathbf{q}}], \quad (2)$$

$$i\hbar\frac{\partial}{\partial t}p_{\mathbf{k}}^{\lambda,\bar{\lambda}}=(\varepsilon_{\mathbf{k}}^{\lambda,\bar{\lambda}}-i\gamma)p_{\mathbf{k}}^{\lambda,\bar{\lambda}}+\Omega_{\mathbf{k}}^{\lambda}(f_{\mathbf{k}}^{e,\lambda}-f_{\mathbf{k}}^{e,\bar{\lambda}})+\sum_{\mathbf{q}}[V_{\lambda,\bar{\lambda}}^{\mathbf{q},\mathbf{k}-\mathbf{q},\mathbf{k}}-(V_{\bar{\lambda},\lambda}^{\mathbf{q},\mathbf{k}-\mathbf{q},\mathbf{k}})^{*}], \quad (3)$$

$$\begin{aligned}i\hbar\frac{\partial}{\partial t}C_{\lambda,\lambda'}^{0,\mathbf{k}',\mathbf{k}}=&(\varepsilon_{\mathbf{k}',0}^{\lambda'}-\varepsilon_{\mathbf{k},0}^{\lambda})C_{\lambda,\lambda'}^{0,\mathbf{k}',\mathbf{k}}+(\Omega_{\mathbf{k}'}^{\lambda'})^{*}C_{\lambda,\bar{\lambda}'}^{0,\mathbf{k}',\mathbf{k}}\\&-\Omega_{\mathbf{k}}^{\lambda}C_{\bar{\lambda},\lambda'}^{0,\mathbf{k}',\mathbf{k}}+[1-f_{\mathbf{k}}^{e,\lambda}-f_{\mathbf{k}}^{h,L}]V_{\lambda,\lambda'}^{0,\mathbf{k}',\mathbf{k}}\\&-[1-f_{\mathbf{k}'}^{e,\lambda'}-f_{\mathbf{k}'}^{h,L}](V_{\lambda',\lambda}^{0,\mathbf{k},\mathbf{k}'})^{*}-V_{\bar{\lambda},\lambda'}^{0,\mathbf{k}',\mathbf{k}}p_{\mathbf{k}}^{\lambda,\bar{\lambda}}\\&+(V_{\bar{\lambda}',\lambda}^{0,\mathbf{k},\mathbf{k}'})^{*}p_{\mathbf{k}'}^{\bar{\lambda}',\lambda'}-i\gamma_{\lambda,\lambda'}^{0,\mathbf{k}',\mathbf{k}}, \end{aligned}\quad (4)$$

where we have applied the main-sum approximation [25,26] and presented the $C_{\lambda,\lambda'}^{\mathbf{q},\mathbf{k}',\mathbf{k}}$ dynamics only for $\mathbf{q}=0$, for simplicity. The notation $\bar{\lambda}$ interchanges the electron-subband index ($\bar{L}=R$ and $\bar{R}=L$) and $\varepsilon_{\mathbf{k},\mathbf{q}}^{\lambda}$ ($\varepsilon_{\mathbf{k}}^{\lambda,\bar{\lambda}}$) is the renormalized electron-hole (electron-electron) energy. Furthermore, $\Omega_{\mathbf{k}}^{\lambda}\equiv D_{\lambda,\bar{\lambda}}E_{\mathrm{THz}}(t)-\sum_{\mathbf{k}'}V_{\mathbf{k}'-\mathbf{k}}^{e,\lambda;e,\bar{\lambda}}p_{\mathbf{k}'}^{\lambda,\bar{\lambda}}$ is the renormalized Rabi frequency, where $E_{\mathrm{THz}}(t)$ is the THz field and $D_{\lambda,\bar{\lambda}}$ is the dipole-matrix element for the electronic intersubband transition ($L\leftrightarrow R$) and $V_{\mathbf{k}}^{\nu,\lambda;\nu',\lambda'}$ defines the Coulomb matrix element between different bands (ν,ν') and subbands (λ,λ'). In general, the charge transfer involves anomalous Coulomb coupling between charge-separated states, but we show in Ref. [16] that such effects are negligible in our structure. The exciton correlations are coupled by the Coulomb interaction through $V_{\lambda,\lambda'}^{\mathbf{q},\mathbf{k}',\mathbf{k}}\equiv\sum_{\mathbf{l}}V_{\mathbf{l}-\mathbf{k}}^{h,L;e,\lambda}C_{\lambda,\lambda'}^{\mathbf{q},\mathbf{k}',\mathbf{l}}$. The two- and three-particle correlations yield scattering [25,26] that is described by γ and $\gamma_{\lambda,\lambda'}^{\mathbf{q},\mathbf{k}',\mathbf{k}}$ within the diffusive model [16,25]. The dephasing used damps intersubband coherences, i.e., currents, with a 1.3 ps decay rate, which is achievable in high-quality QWs [27–29]. To realize efficient population transfer, we apply near-π THz pulses with central frequencies ν_X and ν_e. For a 2 ps duration, pulses have experimentally reasonable field strengths and execute the transport faster than dephasing even when multiple pulses are applied.

We solve Eqs. (1)–(4) numerically to study the realization of the vertical-transport protocols depicted in Fig. 1(b). The initial state of our THz protocol can be flexibly adjusted by utilizing well-known control possibilities of ultrafast optical excitations. As reviewed in Ref. [16], one can prepare a desired initial state by tuning the intensity, photon energy, and duration of the optical excitation, and by applying the THz protocol only after a controllable time delay to allow for a desired amount of exciton formation and/or relaxation controlled by the lattice temperature [30,31]. In this work, we assume low enough temperature where the type-II 1s states dominate the exciton formation; in Ref. [16], we show that our protocols also work at elevated lattice temperatures. For the first two protocols, we consider a situation where all the optical coherences have decayed, the electron-hole density is 10^9 cm^{-2}, all electrons are in the right QW, and 50% of them are bound into indirect (type-II) 1s excitons. The initial plasma-exciton configuration is defined self-consistently as given in Refs. [24,32].

Our first protocol aims at realizing the vertical transfer of unbound electrons across the interface. For this purpose, we employ two sequential THz π pulses whose frequency matches ν_e. The resulting population evolution is shown in Fig. 2(a)(ii). To be precise, we plot the fraction of all electrons $F_{\mathrm{all}}\equiv\sum_{\mathbf{k}}f_{\mathbf{k}}^{e,L}/N_e$ (solid line) and excitons $F_X\equiv\sum_{\mathbf{q},\mathbf{k}}C_{L,L}^{\mathbf{q},\mathbf{k},\mathbf{k}+\mathbf{q}}/N_e$ (shaded area) transported to the left QW; the normalization contains the total number of electrons $N_e\equiv\sum_{\lambda,\mathbf{k}}f_{\mathbf{k}}^{e,\lambda}$. From these, F_{all} denotes the fraction of all transported electrons, whereas F_X and $F_e\equiv F_{\mathrm{all}}-F_X$ determine the respective fractions of transferred electrons transported as excitons or unbound electrons.

Figure 2(a)(ii) show that the first THz pulse yields $F_{\mathrm{all}}=39\%$ (solid line), $F_X=2\%$ (shaded area), and $F_e=37\%$ transport to the left QW. Therefore, 95% of the electrons are transported as unbound electrons, whereas the exciton-bound electrons remain virtually immobile. The same level of selectivity is maintained with the second pulse that transfers the majority of the electrons back to the right QW. In all cases, the deviations from perfect transport can be attributed to the realistic dephasing included in the microscopic calculations.

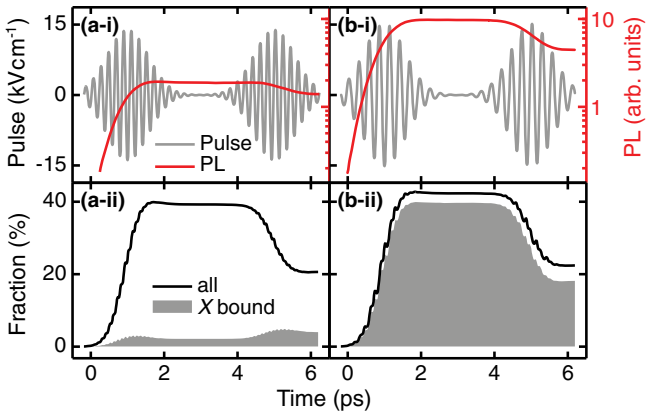

FIG. 2 (color online). Elementary transport protocols. The central frequency of two THz pulses is resonant with the (a) free-electron (ν_e) and (b) exciton (ν_X) transition. (i) The actual THz pulses (gray line) and the emitted photoluminescence (red line) are compared with (ii) the transported fraction of all F_{all} (line) and exciton-bound F_X (shaded area) electrons as a function of time.

In our second protocol, we want to move only the exciton-bound electrons. For this case, we use the same initial state as in Fig. 2(a), but we change the frequency of the THz π pulses to be resonant with exciton transitions ν_X. The results are shown in Fig. 2(b); the first pulse yields $F_{\mathrm{all}} = 42\%$ (solid line), $F_X = 40\%$ (shaded area), and $F_e = 2\%$. This implies that 95% of the transported electrons are bound to excitons, which confirms a high degree of vertical-transport selectivity also in this case.

Whenever electron, hole, or exciton excitations exist in the system, their unavoidable coupling to the quantized optical field yields photoluminescence (PL). We use the luminescence Elliott formula [26] to compute the PL spectrum $I_{\mathrm{PL}}(\omega)$ for the given many-body configuration (see Ref. [16]). The resulting time evolution of $I_{\mathrm{PL}}(\omega_{1s})$ at the direct $1s$ resonance ω_{1s} is shown as a red line in Figs. 2(a)(i) and 2(b)(i) corresponding to ν_e and ν_X excitations, respectively. As we can see, the exciton-transport protocol produces 5 times stronger emission than the electron-transport protocol. Hence, the time-resolved PL could be used in an experiment to follow the details of the THz-induced coherent vertical transfer of electrons or excitons.

In our protocol that realizes pure correlation transport of Fig. 1(b)(iv), we start from a situation where the electron excitation is completely in the right QW and 35% of electron-hole pairs are bound excitons. The exciton fraction is chosen smaller than the ideal 50% to compensate dephasing losses during the transport. To separate the free and exciton-bound electrons to different QWs, we first use a π pulse at frequency ν_e that moves the free electrons to the left QW. Figure 3(a) shows the ν_e pulse as a gray line centered around $t = 1$ ps. The resulting F_{all} (solid line) and F_X (shaded area) are shown in Fig. 3(b). We observe that roughly half of the electrons are moved from right to left during the first THz pulse, whereas the excitons largely remain in the right QW.

To generate pure correlation transport, we then apply a second THz pulse that is centered at $t = 5$ ps. To be precise, we use a THz pulse that is actually a superposition of two pulses, one with frequency ν_e and the other one with ν_X. During this pulse, F_{all} (solid line) remains almost constant, while the exciton correlations are moved spatially from right to left, according to F_X (shaded area) in Fig. 3(b). In other words, the proposed two THz-pulse, two-color excitation protocol delivers an efficient transport of pure correlation in realistic double-QW systems without moving particles. The overall transport is insensitive to the phase between the dual pulse [16].

We have also performed a control computation where the second THz pulse contained only the ν_X part. This scenario, however, not only moves correlations but also the excitons to the left QW. Experimentally, again PL can be used to distinguish exciton transport (only ν_X pulse) from pure correlation transport (ν_e-ν_X superposition pulse). Here, we have to monitor the direct $I_{\mathrm{PL}}(\omega_{1s})$ and the indirect emission $I_{\mathrm{PL}}(\omega_{\mathrm{indir}})$ where ω_{indir} matches the central energy of the indirect luminescence. The red (black) line in Fig. 3(a) shows the direct (indirect) emission for the pure correlation-transport protocol. The final level of the control calculation is shown as horizontal lines. We observe that the pure correlation transport yields 15% lower emission at the direct exciton energy and a 14% larger emission at the indirect exciton. This difference is consistent with the plasma vs exciton correlation contributions [26] to the luminescence, reached with the exciton-transport vs pure correlation-transport protocols. In other words, the correlation transport is distinguishable from the exciton or electron transport through I_{PL}.

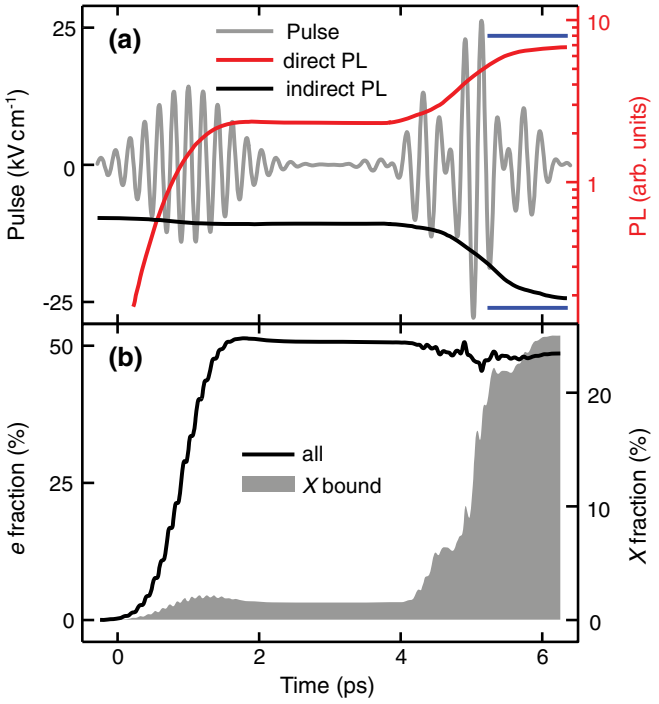

FIG. 3 (color online). Pure correlation-transport protocol. (a) A dual THz pulse (gray line) is shown together with time-resolved luminescence at the direct (red line) and indirect (black line) exciton peak; the vertical lines identify the luminescence levels reached when the second pulse is replaced with the pure exciton-transport protocol. (b) Fraction of all (solid line) vs exciton-bound (shaded area) electrons as a function of time.

In summary, we have demonstrated that one can selectively transport electrons, excitons, or pure exciton correlations through interfaces of realistic double-quantum-well structures by using a suitable sequence of terahertz pulses. We identified a pure correlation transfer protocol which establishes a new scheme to transport quantum-mechanical properties without moving particles. In all transfer schemes, the deviations from ideal operation remain below 6% such that the proposed protocols should be selective enough to characterize and utilize interface properties in nanotechnology applications.

This work is a project of the SFB 1083 funded by the Deutsche Forschungsgemeinschaft (DFG). DFG also supported the work through Grant No. KI 917/2-1. We also acknowledge funding from the Academy of Finland (Projects No. 13140009 and No. 129043) and thank D. Breddermann for his work on an earlier version of the model.

*osmo.vanska@aalto.fi

[1] E. Dupont, P. B. Corkum, H. C. Liu, M. Buchanan, and Z. R. Wasilewski, Phys. Rev. Lett. **74**, 3596 (1995).
[2] R. Atanasov, A. Haché, J. L. P. Hughes, H. M. van Driel, and J. E. Sipe, Phys. Rev. Lett. **76**, 1703 (1996).
[3] A. Haché, Y. Kostoulas, R. Atanasov, J. L. P. Hughes, J. E. Sipe, and H. M. van Driel, Phys. Rev. Lett. **78**, 306 (1997).
[4] L. Costa, M. Betz, M. Spasenović, A. D. Bristow, and H. M. van Driel, Nat. Phys. **3**, 632 (2007).
[5] S. Priyadarshi, K. Pierz, and M. Bieler, Phys. Rev. Lett. **109**, 216601 (2012).
[6] J. Güdde, M. Rohleder, T. Meier, S. W. Koch, and U. Höfer, Science **318**, 1287 (2007).
[7] M. J. Stevens, A. L. Smirl, R. D. R. Bhat, A. Najmaie, J. E. Sipe, and H. M. van Driel, Phys. Rev. Lett. **90**, 136603 (2003).
[8] J. Hübner, W. W. Rühle, M. Klude, D. Hommel, R. D. R. Bhat, J. E. Sipe, and H. M. van Driel, Phys. Rev. Lett. **90**, 216601 (2003).
[9] P. V. Kamat, Acc. Chem. Res. **45**, 1906 (2012).
[10] G. Xing, N. Mathews, S. Sun, S. S. Lim, Y. M. Lam, M. Grätzel, S. Mhaisalkar, and T. C. Sum, Science **342**, 344 (2013).
[11] J. P. Pekola, O.-P. Saira, V. F. Maisi, A. Kemppinen, M. Möttönen, Y. A. Pashkin, and D. V. Averin, Rev. Mod. Phys. **85**, 1421 (2013).
[12] B. S. Williams, Nat. Photonics **1**, 517 (2007).
[13] Y. Yao, A. J. Hoffman, and C. F. Gmachl, Nat. Photonics **6**, 432 (2012).
[14] C. C. Moser, J. M. Keske, K. Warncke, R. S. Farid, and P. L. Dutton, Nature (London) **355**, 796 (1992).
[15] M. Świerczek, E. Cieluch, M. Sarewicz, A. Borek, C. C. Moser, P. L. Dutton, and A. Osyczka, Science **329**, 451 (2010).
[16] See Supplemental Material at http://link.aps.org/supplemental/10.1103/PhysRevLett.114.116802, which includes Refs. [17–21], for details on the model structure, used equations, preparation of initial states, effect of elevated temperatures, and robustness of the protocols.
[17] B. A. Foreman, Phys. Rev. B **49**, 1757 (1994).
[18] I. Vurgaftman, J. Meyer, and L. Ram-Mohan, J. Appl. Phys. **89**, 5815 (2001).
[19] I. Vurgaftman and J. Meyer, J. Appl. Phys. **94**, 3675 (2003).
[20] Ph. Roussignol, M. Gurioli, L. Carraresi, M. Colocci, A. Vinattieri, C. Deparis, J. Massies, and G. Neu, Superlattices Microstruct. **9**, 151 (1991).
[21] O. Buccafusca, J. L. A. Chilla, C. S. Menoni, J. J. Rocca, M. J. Hafich, L. M. Woods, and G. Y. Robinson, Appl. Phys. Lett. **62**, 399 (1993).
[22] K. Hantke, J. D. Heber, C. Schlichenmaier, A. Thränhardt, T. Meier, B. Kunert, K. Volz, W. Stolz, S. W. Koch, and W. W. Rühle, Phys. Rev. B **71**, 165320 (2005).
[23] D. Golde, M. Wagner, D. Stehr, H. Schneider, M. Helm, A. M. Andrews, T. Roch, G. Strasser, M. Kira, and S. W. Koch, Phys. Rev. Lett. **102**, 127403 (2009).
[24] J. T. Steiner, M. Kira, and S. W. Koch, Phys. Rev. B **77**, 165308 (2008).
[25] M. Kira and S. W. Koch, Prog. Quantum Electron. **30**, 155 (2006).
[26] M. Kira and S. W. Koch, *Semiconductor Quantum Optics* (Cambridge University Press, Cambridge, England, 2012).
[27] H. G. Roskos, M. C. Nuss, J. Shah, K. Leo, D. A. B. Miller, A. M. Fox, S. Schmitt-Rink, and K. Köhler, Phys. Rev. Lett. **68**, 2216 (1992).
[28] J. Feldmann, K. Leo, J. Shah, D. A. B. Miller, J. E. Cunningham, T. Meier, G. von Plessen, A. Schulze, P. Thomas, and S. Schmitt-Rink, Phys. Rev. B **46**, 7252 (1992).
[29] P. G. Huggard, C. J. Shaw, S. R. Andrews, J. A. Cluff, and R. Grey, Phys. Rev. Lett. **84**, 1023 (2000).
[30] M. Kira, W. Hoyer, T. Stroucken, and S. W. Koch, Phys. Rev. Lett. **87**, 176401 (2001).
[31] R. A. Kaindl, M. A. Carnahan, D. Hägele, R. Lövenich, and D. S. Chemla, Nature (London) **423**, 734 (2003).
[32] M. Mootz, M. Kira, and S. W. Koch, New J. Phys. **15**, 093040 (2013).